


Lifetime measurements of lowest states in the $\pi g_{7/2} \otimes \nu h_{11/2}$ rotational band in ^{112}I M. M. Giles, D. M. Cullen, B. S. Nara Singh, D. Hodge, M. J. Taylor,* M. J. Mallaburn, N. V. Sosnin, and L. Barber
*School of Physics and Astronomy, Schuster Building, The University of Manchester, Manchester M13 9PL, United Kingdom*J. F. Smith, L. Capponi, and M. Smolen
*School of Engineering and Computing, University of the West of Scotland, Paisley, PA1 2BE, United Kingdom*C. Scholey, P. Rakkila, T. Grahn, H. Badran, A. Girka, P. T. Greenlees, R. Julin, J. Konki, O. Nefodov, P. Ruotsalainen,
M. Sandzelius, J. Sarén, J. Sorri, S. Stolze, J. Uusitalo, J. Pakarinen, P. Papadakis, and J. Partanen
*University of Jyväskylä, Department of Physics, P.O. Box 35, FI-40014, University of Jyväskylä, Finland*T. Braunroth
*Institut für Kernphysik der Universität zu Köln, D-50937 Cologne, Germany*G. G. O'Neill
Department of Physics, Oliver Lodge Laboratory, University of Liverpool, Liverpool, L69 7ZE, United Kingdom (Received 18 April 2018; revised manuscript received 30 August 2018; published 17 October 2018)

A differential-plunger device was used to measure the lifetimes of the lowest states in the $\pi g_{7/2} \otimes \nu h_{11/2}$ rotational band in doubly odd ^{112}I with the $^{58}\text{Ni}(^{58}\text{Ni}, 3pn)$ reaction. A differential decay curve method was performed using the fully shifted and degraded γ -ray intensity measurements as a function of target-to-degrader distance. The lifetimes of the lowest three states in the $\pi g_{7/2} \otimes \nu h_{11/2}$ band in ^{112}I were measured to be 124(30), 130(25), and $\leq 6.5(5)$ ps, respectively. As the lifetimes of successive excited states in a rotational band are expected to decrease with increasing excitation energy, these measurements suggest that the order of the transitions in the established band in ^{112}I may need revising and that the state tentatively assigned to be (7^-) may not belong to the rotational band.

DOI: [10.1103/PhysRevC.98.044315](https://doi.org/10.1103/PhysRevC.98.044315)**I. INTRODUCTION**

The heavy mass isotopes of iodine are known to exhibit features normally associated with collective behavior. For example, a series of strongly coupled rotational bands have been observed in the doubly odd I isotopes [1–4]. The strongly coupled nature of these bands is usually characterized by their signature splitting. Signature splitting can be quantified as the energy of the $M1$ transition linking the strongly coupled rotational bands minus the average energy of the $M1$ transitions directly above and below it [5]. In $^{116-122}\text{I}$ [1,6,7], the strongly coupled rotational bands built upon the $\pi g_{9/2}^{-1} \otimes \nu h_{11/2}$ configuration exhibit a small signature splitting, $S(I^\pi)$ [1,2,5]. For example, in ^{116}I $S(9^-) = 9$ keV and in ^{118}I $S(9^-) = 21$ keV for these $\pi g_{9/2}^{-1} \otimes \nu h_{11/2}$ bands. In contrast, in the lighter mass isotopes, the collective rotational bands are interpreted to be built upon a lower-K proton $g_{7/2}$ configuration coupled to the same neutron $h_{11/2}$ orbital. As a consequence, the strongly coupled nature of the bands in the heavier mass isotopes diminishes in the lighter mass isotopes and larger signature splittings are observed. For example, in ^{114}I the signature

splitting is $S(9^-) \approx 400$ keV [8] and becomes so large in ^{112}I that only one signature of the rotational band is experimentally observed [9].

^{112}I was previously studied by Paul *et al.* [9]. In that work, a series of single-particle states were established at low spins, which were fed by a rotational band at higher spins. The band was interpreted as the favored signature of $\pi g_{7/2} \otimes \nu h_{11/2}$ configuration [9]. The aligned angular momentum for this band showed somewhat irregular behavior at low rotational frequencies as the nucleus went through the simultaneous alignments of both proton and neutron $h_{11/2}$ orbitals [9]. In order to shed some light on the nature of the $\pi g_{7/2} \otimes \nu h_{11/2}$ collective rotational band in ^{112}I , lifetime measurements have been performed in the present work using the Differential Plunger for Unbound Nuclear States (DPUNS) [10].

II. EXPERIMENTAL DETAILS AND ANALYSIS

Excited states in ^{112}I were populated with the $^{58}\text{Ni}(^{58}\text{Ni}, 3pn)$ fusion-evaporation reaction. The experiment employed a 230-MeV 4-pnA ^{58}Ni beam, produced with the K130 cyclotron at the Accelerator Laboratory of the University of Jyväskylä, which was used to bombard a 1.1-mg/cm^2 ^{58}Ni target for 12 days. A 1.5-mg/cm^2 ^{24}Mg

*Present address: Division of Cancer Sciences, University of Manchester, Manchester, M20 4BX, United Kingdom.

degrader foil was placed downstream from the target. Subsequently, the degraded recoils traveled through the recoil ion transport unit (RITU) [11], triggering a multiwire proportional counter (MWPC) before they were implanted into a double-sided silicon strip detector (DSSD) [12]. RITU was used to transport the recoiling evaporation products, or recoils, to the focal plane while suppressing any primary beam.

The target was mounted at the center of JUROGAM-II γ -ray spectrometer, inside the DPUNS [10], along with the ^{24}Mg degrader foil. The JUROGAM-II array was used to measure the γ -ray intensities [13]. JUROGAM-II consisted of 39 Compton-suppressed germanium detectors arranged into four rings, with angles $\theta = 76^\circ, 105^\circ, 134^\circ$, and 158° with respect to the beam axis. Rings 1 and 2 consisted of 5 and 10 EUROGAM phase I-type detectors at angles of 158° and 134° , respectively [14]. The remaining two rings each contained 12 Clover detectors at $\theta = 76^\circ$ and $\theta = 105^\circ$ [15]. A total data readout (TDR) system recorded all detector events with a time stamp [16], allowing the GRAIN package to be used for offline analysis [17].

The degrader foil inside DPUNS reduced the velocity of the recoils, which split the intensity of each detected γ -ray transition into two Doppler-shifted components, $I^s(x)$ and $I^d(x)$. Here $I^s(x)$ is the component peak intensity corresponding to decays before the degrader foil (fully shifted), and $I^d(x)$ is the component peak intensity corresponding to decays after the degrader foil (degraded). The differential decay curve method (DDCM) was used on these component peak intensities as a function of plunger distance, $x = 135, 210, 300, 590$, and $3000 \mu\text{m}$, to deduce the lifetimes of the states of interest [18,19].

To remove the effect of potential side-feeding from higher lying states, a gate on the fully-shifted (fs) component of the γ ray directly above the level of interest was placed using the *gf3* software package [20,21]. The lifetime was determined by using Eq. (1) [18],

$$\tau(x) = \frac{1}{v} \frac{\{I_{\text{feed}}^s, I_{\text{dec}}^d\}(x)}{\frac{d}{dx} \{I_{\text{feed}}^s, I_{\text{dec}}^s\}(x)}. \quad (1)$$

Here, v is the average recoil velocity and $\{I_{\text{feed}}^s, I_{\text{dec}}^d\}$ denotes the intensity of the degraded component of the γ ray from the decay of the level of interest measured in coincidence with the fully shifted peak of the γ ray from the decay of the direct feeding level. When a coincidence gate was set on a transition C above the level of interest, but not directly above (see Sec. III A), Eq. (2) was used:

$$\tau(x) = \frac{1}{v} \frac{\{I_C^s, I_{\text{dec}}^d\}(x) - \{I_C^s, I_B^d\}(x) \frac{\{I_C, I_{\text{dec}}\}}{\{I_C, I_B\}}}{\frac{d}{dx} \{I_{\text{feed}}^s, I_{\text{dec}}^s\}(x)}, \quad (2)$$

where $\{I_C^s, I_B^d\}$ is the intensity of the degraded components of transition B between the gate and the the state of interest. The term $\frac{\{I_C, I_{\text{dec}}\}}{\{I_C, I_B\}}$, which is often called α [18], reflects any intensity difference between the feeding and depopulating transitions.

As ^{112}I was a weakly populated channel in the $^{58}\text{Ni}(^{58}\text{Ni}, 3pn)$ reaction, a γ -ray coincidence gate was first required to select the ^{112}I nuclei from other reaction products.

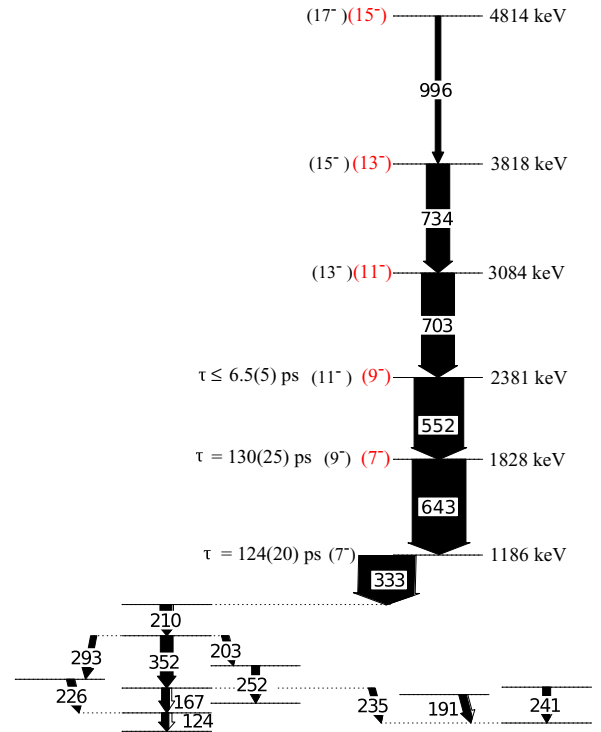


FIG. 1. The level scheme observed in this work for ^{112}I showing the low-spin single-particle levels and the higher lying single-signature rotational band. The level scheme is in agreement with Ref. [9] apart from the ordering of the 552- and 643-keV transitions which have been reversed in the present work (see Sec. IV). Proposed spin assignments from Ref. [9] are shown in black, and proposed assignments from this work are shown in red.

This selection gate set a requirement that only γ -ray events in coincidence with both components of either the 203- or 210-keV γ rays at the top of the lower spin single-particle structure in ^{112}I (see Fig. 1) were used in the subsequent γ - γ lifetime matrices. These gated two-dimensional (2D) γ - γ matrices were produced for ring 1 versus any detector in ring 1 or ring 2 (all) as a function of plunger distance. Likewise, 2D gated matrices were produced for ring 2 versus any detector in ring 1 or ring 2. These matrices are referred to as ring 1-all, and ring 2-all, respectively. In these matrices, a second gate on the fully-shifted component of the γ ray directly above the level of interest was then applied to remove potential side feeding. This gate was applied onto the all axis in order to produce the final double-gated spectra projected onto the ring 1 or ring 2 axis, which were used for to obtain the lifetime of interest. A single gate on the fully-shifted component on the all axis was used, as the Doppler shifts in rings 1 and 2 were very similar. In this work, the double gated spectra are denoted $(E_{\gamma}^{\text{below}}/E_{\gamma}^{\text{above}})$.

$I^s(x)$ and $I^d(x)$ were measured and normalized to the total number of counts in the x projection of the gated 2D matrix for a given x . A piecewise second-order polynomial was fitted to the fully-shifted component as a function of distance. The derivative of this was fitted to the degraded components and

TABLE I. The γ -ray energies and relative intensities of the lower transitions in the rotational band measured in this work from a double-gated spectrum, using the gates 203 or 210 keV with the 333-keV γ -ray transition.

E_γ (keV)	I_γ
551.5(3)	98(4)
642.7(2)	100(3)
702.5(2)	59(4)
733.7(3)	35(2)
996.7(4)	19(2)

Eq. (1) was used to calculate the lifetime at each of the target-to-degrader distances [19].

III. RESULTS

Figure 1 shows a partial level scheme of ^{112}I from this work, showing the single-particle states at low excitation energy and the collective band emerging at higher excitation energies. The observed sequence is in agreement with previous studies [9] apart from the order of the first two states in the rotational band (see Sec. IV). The widths of the arrows correspond to the efficiency corrected intensities measured in this experiment. The level scheme was constructed using data from clover versus clover gated γ - γ spectra, which combined the data from all distances. These detector rings are at 76° and 105° and hence the γ -ray Doppler shift is small. The measured γ -ray energies and intensities of the rotational structure from these gated γ - γ matrices are given in Table I.

Figure 2 shows typical spectra obtained for the band of interest, used to deduce the level scheme in Fig. 1. Figure 2(a) shows a projection of the JUROGAM-II clover versus clover γ - γ fully shifted matrix, for all distances combined for multiplicity 3 or higher events, where at least one of the events was detected in coincidence with the 203- or 210-keV transitions. The ^{112}I transitions are labeled with their γ -ray energies whereas γ rays originating from other reaction channels are labeled with symbols, defined in the legend. The main contaminants, with $A \approx 80$, were produced from ^{58}Ni reactions with the ^{24}Mg degrader foil. Figures 2(b) and 2(c) were created using the same gated γ - γ matrix and show decays in coincidence with the 552- and 703-keV transitions, respectively. The data were sorted using the measured recoil velocity of $v/c = 0.038(2)$ after leaving the target (fully shifted). The measured velocity after passing through the degrader (degraded) was $v/c = 0.018(2)$.

A. Lifetime analysis

In order to extract fully shifted and degraded component peak intensities as a function of target-to-degrader distance to perform a lifetime analysis, the fully shifted and degraded components of the γ -ray transitions depopulating the states of interest were measured using the gated background subtracted matrices of ring 1-all and ring 2-all. Gaussian fits were made to the fully shifted and degraded components. To reduce the

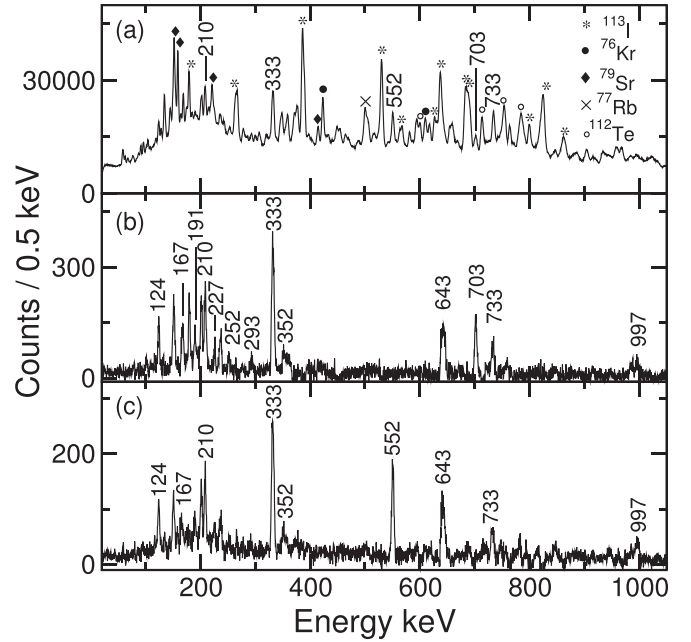


FIG. 2. ^{112}I spectra obtained from JUROGAM-II clover vs clover γ - γ matrices. (a) Single-gated projection using gates on both the 210- and the 203-keV transitions. ^{112}I transitions are labeled with their energies and contaminants are labeled with symbols given in the legend. Panel (b) shows a double-gated spectrum, using the same gate as panel (a) in coincidence with an additional 552-keV gate. Panel (c) is also a double-gated spectrum using the gate from (a) and an additional gate on the 703-keV transition.

fitting errors, the widths and centroids of the peaks were fixed. The fully shifted widths and centroids were fixed using the $3000\ \mu\text{m}$ distance and the degraded widths and centroids were fixed using the $135\ \mu\text{m}$ distance. At these respective distances, only one of the fully shifted or degraded components were present. Table II shows the fitted widths and centroids for 333- and 643-keV transitions.

1. Lifetime of the state which decays by the 333-keV transition

To examine the lifetime of the state at 1186 keV in ^{112}I , the 2D γ - γ ring 1-all and ring 2-all matrices were used to produce $((203, 210)/643_{f_s})$ gated spectra for each plunger distance.

TABLE II. The centroids (C) and widths (W) of the fully shifted and degraded components of the 333- and 643-keV transitions in ^{112}I from the ring 1-all and ring 2-all double-gated matrices. The double gates $((210, 203)/643_{f_s})$ and $((210, 203)/552_{f_s})$ are used, respectively.

γ -ray transition	Ring 1		Ring 2	
	C (keV)	W (keV)	C (keV)	W (keV)
333 keV (Shifted)	332.8	3.7	332.8	3.8
333 keV (Degraded)	337.8	3.6	336.8	3.3
643 keV (Shifted)	642.6	5.8	642.7	4.1
643 keV (Degraded)	653.2	4.1	650.5	3.6

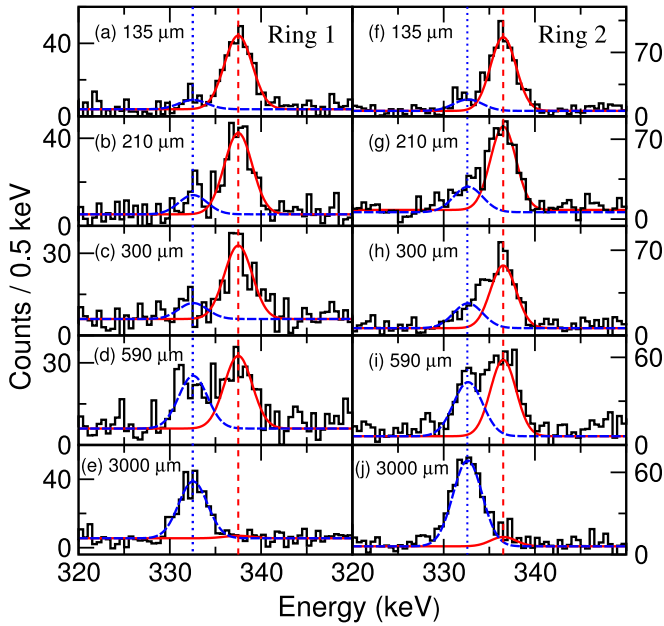


FIG. 3. ^{112}I double-gated spectra from the ring 1-all (left) and ring 2-all (right) matrices, using gates on both components of the 203- or 210-keV γ -ray transitions with the fully-shifted component of the 643-keV γ -ray transition. The fully shifted (blue-dashed) and degraded (red-solid) components of the 333-keV peak for ring 1 and ring 2 are shown for target-to-degrader distances 135 to 3000 μm , for panels (a) to (e) and (f) to (j). The presented spectra are Doppler corrected with respect to the recoil velocity after the target ($v/c = 0.038(2)\%$).

These spectra are shown in Fig. 3. The measured centroids of the fully shifted and degraded components are shown in dotted and dashed vertical lines, respectively. The normalized intensities of the two components of the 333- and 643-keV transitions are given at each distance in Table III.

The differential decay curve method was used to find the lifetime of the state decaying by the 333-keV γ -ray transition. Figures 4(a) and 4(d) show the lifetime of the state decaying via the 333-keV γ -ray transition for target-to-degrader distances in the region of sensitivity for ring 1 and ring 2, respectively. Figures 4(b) and 4(e) show the normalized component peak intensities of the fully-shifted component as a function of distance for rings 1 and 2, respectively, which were used to deduce the lifetimes of the states. Figures 4(c) and 4(f) show the normalized peak intensities of the degraded

TABLE III. The normalized intensities of the fully shifted and degraded γ -ray peak components of the 333- and 643-keV transitions in ^{112}I for both ring 1 and ring 2 detectors, using the double gates $((203, 210)/643_{fs})$ and $((203, 210)/552_{fs})$, respectively.

Distance (μm)	Ring 1 (134°)				Ring 2 (158°)			
	I_{333}^s	I_{333}^d	I_{643}^s	I_{643}^d	I_{333}^s	I_{333}^d	I_{643}^s	I_{643}^d
135	40(10)	310(20)	20(10)	150(30)	100(20)	570(60)	70(20)	260(40)
210	60(20)	260(30)	40(10)	120(20)	150(20)	440(40)	60(10)	230(30)
300	40(15)	190(20)	40(10)	140(20)	190(30)	420(50)	50(20)	210(30)
590	100(10)	140(15)	80(10)	120(20)	250(30)	320(40)	140(20)	150(20)
3000	230(30)	10(10)	170(20)	24(10)	550(60)	50(20)	230(30)	20(10)

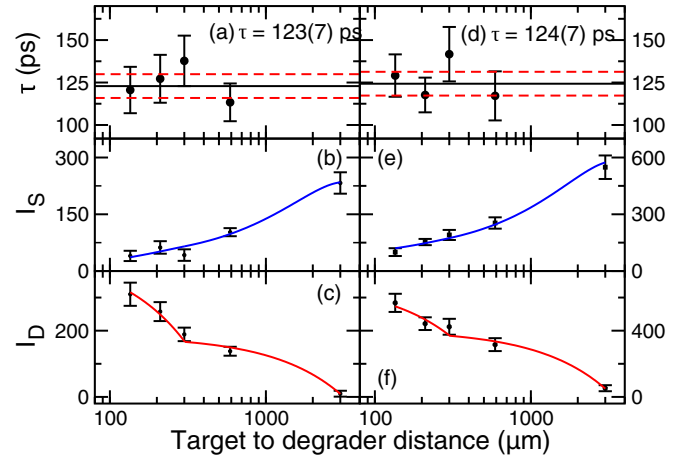


FIG. 4. (a) Lifetime analysis of the state in ^{112}I decaying via the 333-keV transition, based on DDCM using the ring 1 (left) and ring 2 (right) detectors. The intensities of the fully-shifted components of the 333-keV γ ray as a function of distance are shown in panels (b) and (e), with the degraded components in panels (c) and (f).

component as a function of distance. The weighted mean lifetimes calculated from ring 1 and ring 2 of $\tau = 123(7)$ ps and $\tau = 124(7)$ ps, respectively, are also shown.

The uncertainty shown on the lifetime fits is the weighted uncertainty of the lifetimes calculated at each distance. As the number of data points in the region of sensitivity was small, the fit to the data has relatively large uncertainties. This is partly due to not having an “anchor” point at small distances to constrain the fit. In this case, the weighted average of the lifetime from the four distance measurements results in an underestimate of the true lifetime uncertainty. A more accurate estimate of the uncertainty was made by varying the fit on the data to increase and decrease the χ^2 by 0.5, which gave an error of 20 ps. In view of this, the average lifetime of the state decaying via the 333-keV E1 γ -ray transition, using both ring 1 and ring 2, was deduced to be $\tau = 124(20)$ ps.

2. Lifetime of the state decaying by the 643-keV transition

Figure 5 shows the $((203, 210)/552_{fs})$ double-gated spectra used to obtain the intensities of the two components of the 643-keV transition. The intensities of each component at each distance are given in Table III, for ring 1 (left) and ring 2 (right).

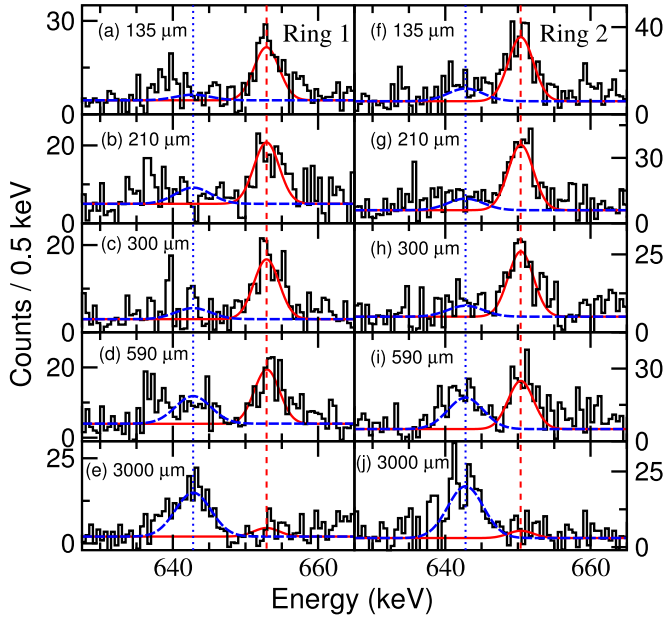


FIG. 5. ^{112}I double-gated spectra projected from the ring 1-all and ring 2-all matrices, using gates on both components of the 203- or 210-keV γ -ray transitions with the fully-shifted component of the 552-keV γ -ray transition. The fully shifted (blue-dashed) and degraded (red-solid) components of the 643-keV peak for ring 1 and ring 2 (left and right) are shown for target-to-degrader distances 135 to 3000 μm , for panels (a) to (e) and (f) to (j). The presented spectra are Doppler corrected with respect to the recoil velocity after the target ($v/c = 0.038(2)\%$).

Figures 6(a) and 6(d) show the lifetime of the state decaying by the 643-keV γ -ray transition for plunger distances in the region of sensitivity for ring 1 and ring 2, respectively. Figures 6(b) and 6(e) show the normalized intensities of the

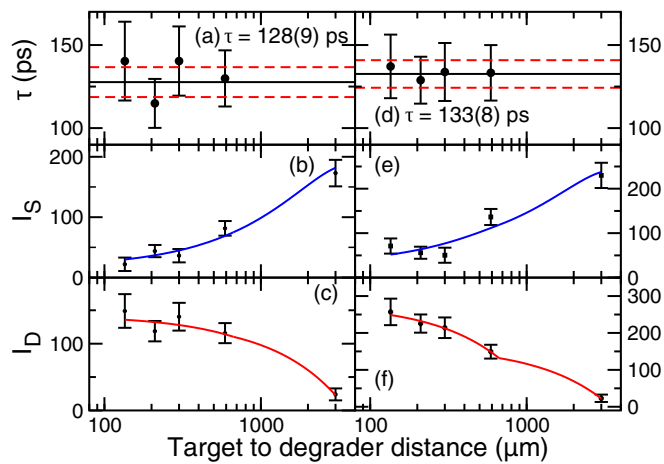


FIG. 6. (a) and (d) Lifetime analysis of the state in ^{112}I decaying by the 643-keV transition, based on DDCM using the ring 1 (left) and ring 2 (right) detectors. The intensities of the fully-shifted components of the 643-keV γ ray as function of distance are shown in panels (b) and (e), with the degraded components in panels (c) and (f).

fully-shifted component of the 643-keV γ -ray as a function of distance for rings 1 and 2, respectively. The solid lines show a least squares fit to the data. Figures 6(c) and 6(f) show the normalized intensities of the degraded component of the 643-keV γ ray as a function of distance with a least squares fit to the data (solid line). The weighted mean lifetimes for ring 1 and ring 2 of $\tau = 128(9)$ ps and $\tau = 133(8)$ ps are also shown.

As previously discussed, to better estimate the true error on the lifetime measurement for this state, the fit on the data was varied to increase and decrease the χ^2 by 0.5. The average lifetime of the state decaying by the 643-keV γ -ray was thereby deduced to be $\tau = 130(25)$ ps.

It should be noted that the γ -ray intensities of the 552- and 643-keV transitions from the lowest two states in the band are equal to each other within one standard deviation of their measured uncertainties in both the present and previous experiments [9]. This equality of transition intensities for the lowest two transitions in the band means that their order is somewhat ambiguous. This ambiguity could potentially affect the lifetime measurement, as in order to remove potential side feeding, the coincidence gate must be set above the transition of interest. For the lifetime analysis of the 1828-keV state shown in Fig. 1, both possible transition orderings for the 552- and 643-keV transitions were considered.

In the original level scheme proposed by Paul *et al.* [9], the 703-keV γ -ray directly feeds the state decaying by the 643-keV transition. For this level ordering, a lifetime analysis for the state decaying by the the 643-keV transition was performed using a gate from above on the fully-shifted component of the 703-keV transition, which resulted in a lifetime of 135(20) ps.

In our revised level scheme, the 552-keV transition is the direct feeder of the 1828-keV state, and hence for the lifetime analysis of the 1828-keV state a gate was effectively placed on the fully-shifted component of the 552-keV transition and the lifetime was found to be 130(25) ps. In both approaches, Eq. (2) was used but the term $\{I_C^s, I_B^d\}(x) \approx 0$. Both measured lifetime values are consistent within one standard deviation.

The agreement in the lifetime values of the 1828-keV state from the two different gates distinguishes between the ordering presented in Fig. 1 and the ordering presented in Ref. [9]. If the original ordering from Ref. [9] remained unchanged, our gate on the fully-shifted component of the 552-keV transition would have yielded no events in the degraded component of the 643-keV transition because the gate would have been below set the state of interest. The spectra produced using the gate on the fully-shifted component of the 552-keV transition is shown in Fig. 5 and events in both components of the 643-keV transition are observed. Using a similar logic, if the ordering in Fig. 1 is assumed, then a gate placed on the fully-shifted component of the 643-keV transition should produce no events in the degraded component of the 552-keV transition because the gate is set below the state of interest. In Fig. 7, it can be seen that no intensity in the degraded component of the 552-keV transition is observed at any target-to-degrader distance. These two points demonstrate that the 552-keV transition lies above the 643-keV transition. This is further discussed in Sec. IV A.

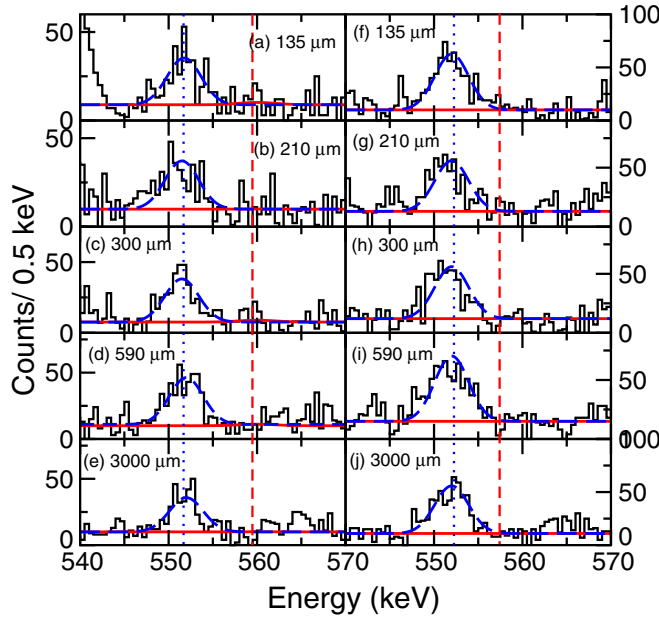


FIG. 7. ^{112}I double-gated spectra from the ring 1-all (left) and ring 2-all (right) matrices, using gates on both components of the 203- or 210-keV γ -ray transitions with the fully-shifted component of the 643-keV γ -ray transition. The fully shifted (blue-dashed) components of the 552-keV peak for ring 1 and ring 2 are shown. No intensity in the degraded component of the 552-keV peak is observed at any distance. The presented spectra are Doppler corrected with respect to the recoil velocity after the target ($v/c = 0.038(2)\%$).

3. Lifetime of the state decaying by the 552-keV transition

An attempt was made to deduce the lifetime of the state decaying via the 552-keV γ -ray transition. However, only a small component in the degraded peak of this transition was observed at the shortest 135 μm target-to-degrader distance; see Fig. 8. No intensity in the degraded peak was observed for larger distances.

Using the ratio of degraded to fully shifted intensities at 135 μm , an upper limit of $\tau \leq 6.5$ ps was de-

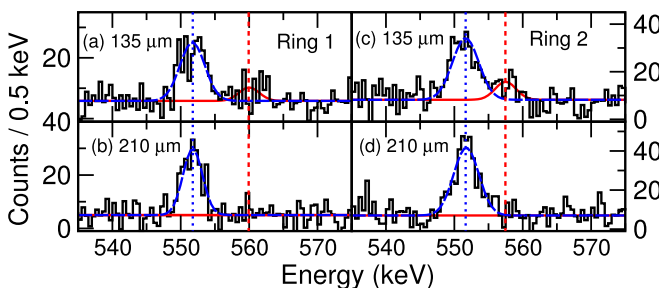


FIG. 8. ^{112}I double-gated spectra from the ring 1-all (left) and ring 2-all (right) matrices, using gates on both components of the 203- or 210-keV γ -ray transitions with the fully-shifted component of the 703-keV γ -ray transition. The fully shifted (blue-dashed) and degraded (red-solid) components of the 552-keV peak for ring 1 and ring 2 are shown for target-to-degrader distances of 135 and 210 μm . The presented spectra are Doppler corrected with respect to the recoil velocity after the target ($v/c = 0.038(2)\%$).

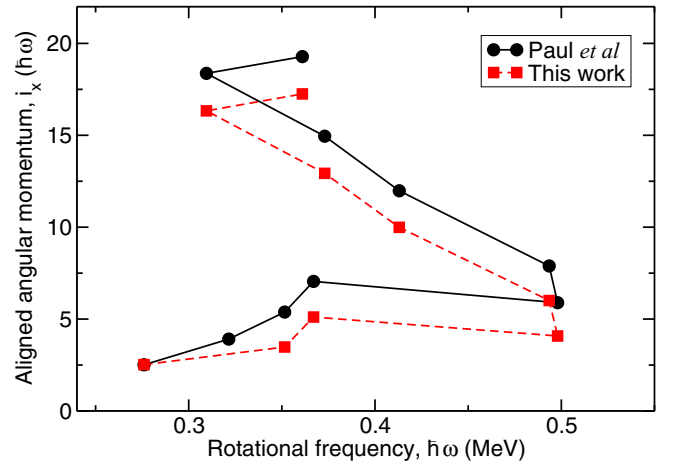


FIG. 9. Aligned angular momentum or alignment, i_x , for the band structure in ^{112}I from Ref. [9] in black solid line and from this work (red-dashed line) with the first two states in the band reordered (see text for details). Harris parameters [24] $\mathcal{J}_0 = 15\hbar^2 \text{MeV}^{-1}$ and $\mathcal{J}_1 = 25\hbar^4 \text{MeV}^{-3}$ have been subtracted from each band plotted in the figure.

duced for the lifetime of the state decaying via the 552-keV transition. Shorter target-to-degrader distances would be required to firmly establish the lifetime of this state.

IV. DISCUSSION

In the previous work [9], cranked shell model (CSM) and total Routhian surface calculations (TRS) [22,23] were performed in order to interpret the underlying configuration of the single rotational band in ^{112}I . These calculations predicted that the rotational structure in ^{112}I had a $\pi g_{7/2} \otimes \nu h_{11/2}$ configuration at low rotational frequencies. Additionally, in the previous work, directional correlation (DCO) ratios for several γ -ray transitions were measured. For example, the 643-keV transition was reasoned to be an $E2$ transition from the DCO ratio of 1.04(8) and the 333-keV transition was reasoned to be a dipole transition with some possible $E2$ mixing from the measured DCO ratio of 0.64(7) [9]. Based on these DCO ratios along with the TRS calculations, the state at 1186 keV was assigned to be the (7^-) bandhead of the $\pi g_{7/2} \otimes \nu h_{11/2}$ configuration [9]. From Ref. [9], the lower lying levels are due to single-particle structure.

A. Ordering of the states in the $\pi g_{7/2} \otimes \nu h_{11/2}$ band

The aligned angular momentum or alignment, i_x , for the $\pi g_{7/2} \otimes \nu h_{11/2}$ band is plotted (black solid line) in Fig. 9 from Ref. [9].

The large ($\approx 20\hbar$) gain in aligned angular momentum around rotational frequencies $\hbar\omega \approx 0.4$ MeV was interpreted to be due to simultaneous alignment of both proton and neutron in the $h_{11/2}$ orbitals [9]. Hence, the configuration of the structure at high rotational frequencies was deduced to be based upon a $\pi g_{7/2}[h_{11/2}]^2 \otimes \nu[h_{11/2}]^3$ configuration [9].

This configuration was the basis of the spin assignment for the band.

In the previous work [9], the γ -ray transitions in the rotational structure were ordered based on their intensities and coincidence relationships alone. In the present work, lifetimes of several of the states in this $\pi g_{7/2} \otimes \nu h_{11/2}$ rotational band have been measured for the first time. These lifetimes, and measured γ -ray coincidence relations between fully shifted and degraded components of consecutive transitions, suggested a reordering of two transitions in the band was required compared to Ref. [9]. Figure 5 shows the γ rays from the 643-keV transition in coincidence with the fully-shifted component of the 552-keV transition. Events in both the fully shifted and degraded components of the 643-keV transition are observed. The degraded component of the 643-keV transition can only be in coincidence with the fully-shifted component of the 552-keV transition if the 643-keV transition occurs after the 552-keV transition in time, supporting the ordering in Fig. 1. In a similar way, Fig. 7 shows the γ rays from the 552-keV transition in coincidence with the fully-shifted component of the 643-keV transition. No events in the degraded component of the 552-keV transition are observed at any distance. This suggests the 552-keV transition occurs before the 643-keV transition, again supporting the ordering presented in Fig. 1. This lifetime evidence supports a reordering of the 552- and the 643-keV transitions compared to the level scheme in Ref. [9]. However, it must be noted that the short lifetime of the state at 2381 keV would also produce spectra with no events in the degraded component of the 552-keV transition. Figure 1 shows the revised level scheme for the $\pi g_{7/2} \otimes \nu h_{11/2}$ rotational band based on the evidence presented in Sec. III A.

The long lifetime of the state at 1828-keV indicates that the state at 1186-keV has non-collective or hindered single-particle behavior (see Sec. IV B). This suggests that the 1186-keV state may not belong to the band. Thus, based on our lifetime measurements, we propose that the (7^-) bandhead may in fact be higher at 1828 keV. The rotational band is then built upon this (7^-) bandhead state at 1828-keV as suggested in Ref. [9]. Hence, Fig. 1 also shows revised tentative spin assignments for the rotational band.

Figure 9 shows the aligned angular momentum for the reordered structure in ^{112}I (red squares) where the first two states in the rotational band have been reversed in accordance with our lifetime measurements and the state at 1186 keV is no longer part of the band. The new tentative spin assignments from Fig. 1 are used. The revised alignment plot affects the alignment pattern of the lowest two states and does not change any of the proposed configurations and band crossings concluded in Ref. [9].

B. A comparison of predicted and experimentally deduced deformations

In the previous work [9], TRS calculations for the $\pi g_{7/2} \otimes \nu h_{11/2}$ configuration below the crossing predicted a quadrupole deformation and triaxiality, $(\beta_2, \gamma) \approx (0.175, 9^\circ)$. Above the crossing, these TRS calculations predict a more deformed and triaxial shape with $(\beta_2, \gamma) \approx (0.22, >15^\circ)$ for the $\pi g_{7/2}[h_{11/2}]^2 \otimes \nu[h_{11/2}]^3$ configuration [9]. The TRS calculations showed a trend of increasing triaxiality with increasing rotational frequency or seniority [9].

The deformation deduced from the lifetime measurement of the 643-keV transition in the present work was $\beta_2 = 0.021(8)$ [25]. This is 10 times smaller than the value predicted by the TRS calculations. Hence it was concluded that the state at 1186 keV does not form a part of the band. The deformation obtained from the limit on the lifetime of the 552-keV transition was $\beta_2 \geq 0.13$ [25]. This deformation is more comparable to that predicted from the TRS calculations for the $\pi g_{7/2} \otimes \nu h_{11/2}$ configuration, although the experimental value is only a lower limit. A more thorough lifetime experiment focused on ^{112}I would be required in order to make a full comparison with TRS.

V. CONCLUSIONS

In summary, the new lifetime measurements made in the present work reveal that the structure of the proposed rotational band in ^{112}I is more complicated than intensity and coincidence measurements alone reveal. Although the majority of the level scheme in this work is consistent with that established in Ref. [9], the lifetime measurements suggest a reordering of the lowest two transitions in the band. The relatively long lifetime of the state at 1828-keV suggest that it is the (7^-) bandhead. Hence, new tentative spin assignments have been given on the assumption that the state at 1828 keV is the true bandhead of the $\pi g_{7/2} \otimes \nu h_{11/2}$ band. Higher statistics data from γ -ray spectroscopy or an additional lifetime experiment, optimized for ^{112}I , would be required to help fully confirm the revised level ordering presented here.

ACKNOWLEDGMENTS

This work was supported by the EU 7th Framework Programme, Integrating Activities Transnational Access, Project No. 262010 ENSAR, and by the Academy of Finland under the Finnish Centre of Excellence Programme (Nuclear and Accelerator Based Physics Programme at JYFL). The authors acknowledge GAMMAPOOL support for the JUROGAM detectors and M.M.G., D.M.C., B.S.N.S., D.H., M.J.T., M.J.M., J.F.S., and M.S. acknowledge support of the Science and Technology Facilities Council, Grant No. ST/L005794/1.

- [1] C.-B. Moon, T. Komatsubara, and K. Furuno, Band structures in ^{116}I , *Nucl. Phys. A* **730**, 3 (2004).
 [2] E. S. Paul, D. B. Fossan, K. Hauschild, I. M. Hibbert, H. Schnare, J. M. Sears, I. Thorslund, R. Wadsworth, A. N. Wilson,

and J. N. Wilson, High-spin rotational bands in doubly odd ^{118}I , *J. Phys. G: Nucl. Part. Phys.* **22**, 653 (1996).

- [3] C.-B. Moon, G. Dracoulis, R. A. Bark, A. Byrne, P. Davidson, T. Kibedi, G. Lane, and A. Wilson, Various isomers

- in doubly odd I isotopes, *J. Korean Phys. Soc.* **59**, 1525 (2011).
- [4] P. Singh, S. Nag, K. Selvakumar, A. K. Singh, I. Ragnarsson, A. Bisoi, A. Goswami, S. Bhattacharya, S. Kumar, K. Singh *et al.*, High-spin spectroscopy of ^{122}I , *Phys. Rev. C* **85**, 054311 (2012).
- [5] R. Zheng, S. Zhu, N. Cheng, and J. Wen, Systematics of signature inversion in odd-odd nuclei in the mass regions $a = 80$ and $a = 160$, *Phys. Rev. C* **64**, 014313 (2001).
- [6] E. S. Paul, P. J. Woods, T. Davinson, R. D. Page, P. J. Sellin, C. W. Beausang, R. M. Clark, R. A. Cunningham, S. A. Forbes, D. B. Fossan *et al.*, In-beam γ -ray spectroscopy above ^{100}Sn using the new technique of recoil decay tagging, *Phys. Rev. C* **51**, 78 (1995).
- [7] M. A. Quader, W. F. Piel, S. Vajda, W. A. Watson, F. C. Yang, and D. B. Fossan, Proton-hole-induced bands in odd-odd $^{116,118,120,122}\text{I}$ nuclides, *Phys. Rev. C* **30**, 1772 (1984).
- [8] E. S. Paul, H. R. Andrews, T. E. Drake, J. DeGraaf, V. P. Janzen, S. Pilotte, D. C. Radford, and D. Ward, High-spin states in doubly odd ^{114}I , *Phys. Rev. C* **52**, 1691 (1995).
- [9] E. S. Paul, C. W. Beausang, R. M. Clark, R. A. Cunningham, D. B. Fossan, A. Gizon, J. Gizon, K. Hauschild, I. M. Hibbert, A. N. James *et al.*, High-spin states in doubly odd ^{112}I , *J. Phys. G: Nucl. Part. Phys.* **21**, 1001 (1995).
- [10] M. J. Taylor, D. M. Cullen, A. J. Smith, A. McFarlane, V. Twist, G. A. Alharshan, M. G. Procter, T. Braunroth, A. Dewald, E. Ellinger *et al.*, A new differentially pumped plunger device to measure excited-state lifetimes in proton emitting nuclei, *Nucl. Instrum. Methods Phys. Res., Sect. A* **707**, 143 (2013).
- [11] M. Leino, J. yst, T. Enqvist, P. Heikkinen, A. Jokinen, M. Nurmia, A. Ostrowski, W. Trzaska, J. Uusitalo, K. Eskola, P. Armbruster, and V. Ninov, Gas-filled recoil separator for studies of heavy elements, *Nucl. Instrum. Methods Phys. Res., Sect. B* **99**, 653 (1995).
- [12] R. D. Page, A. N. Andreyev, D. E. Appelbe, P. A. Butler, S. J. Freeman, P. T. Greenlees, R.-D. Herzberg, D. G. Jenkins, G. D. Jones, P. Jones *et al.*, The {GREAT} spectrometer, *Nucl. Instrum. Methods Phys. Res., Sect. B* **204**, 634 (2003).
- [13] C. W. Beausang and J. Simpson, Large arrays of escape suppressed spectrometers for nuclear structure experiments, *J. Phys. G: Nucl. Part. Phys.* **22**, 527 (1996).
- [14] C. W. Beausang, S. A. Forbes, P. Fallon, P. J. Nolan, P. J. Twin, J. N. Mo, J. C. Lisle, M. A. Bentley, J. Simpson, F. A. Beck, D. Curien, G. de France, G. Duchêne, and D. Popescu, Measurements on prototype Ge and {BGO} detectors for the Eurogam array, *Nucl. Instrum. Methods Phys. Res., Sect. A* **313**, 37 (1992).
- [15] G. Duchêne, F. A. Beck, P. J. Twin, G. de France, D. Curien, L. Han, C. W. Beausang, M. A. Bentley, P. J. Nolan, and J. Simpson, The Clover: A new generation of composite Ge detectors, *Nucl. Instrum. Methods Phys. Res., Sect. A* **432**, 90 (1999).
- [16] I. H. Lazarus, D. E. Appelbe, P. A. Butler, P. J. Coleman-Smith, J. R. Cresswell, S. J. Freeman, R. D. Herzberg, I. Hibbert, D. T. Joss, S. C. Letts *et al.*, The great triggerless total data readout method, *IEEE Trans. Nucl. Sci.* **48**, 567 (2001).
- [17] P. Rakhila, Grain a Java data analysis system for total data readout, *Nucl. Instrum. Methods Phys. Res., Sect. A* **595**, 637 (2008).
- [18] A. Dewald, O. Müller, and P. Petkov, Developing the recoil distance Doppler-shift technique towards a versatile tool for lifetime measurements of excited nuclear states, *Prog. Part. Nucl. Phys.* **67**, 786 (2012).
- [19] A. Dewald, S. Harissopulos, and P. von Brentano, The differential plunger and the differential decay curve method for the analysis of recoil distance Doppler-shift data, *Z. Phys. A* **334**, 163 (1989).
- [20] D. Radford, Background subtraction from in-beam HPGE coincidence data sets, *Nucl. Instrum. Methods Phys. Res., Sect. A* **361**, 306 (1995).
- [21] D. Radford, Escl8r and levit8r: Software for interactive graphical analysis of HPGE coincidence data sets, *Nucl. Instrum. Methods Phys. Res., Sect. A* **361**, 297 (1995).
- [22] W. Nazarewicz, G. Leander, and J. Dudek, Octupole shapes and shape changes at high spins in Ra and Th nuclei, *Nucl. Phys. A* **467**, 437 (1987).
- [23] W. Nazarewicz, R. Wyss, and A. Johnson, Structure of superdeformed bands in the $A \approx 150$ mass region, *Nucl. Phys. A* **503**, 285 (1989).
- [24] S. M. Harris, Higher order corrections to the cranking model, *Phys. Rev.* **138**, B509 (1965).
- [25] R. B. Firestone, C. M. Baglin, and S. Chu, *Table of Isotopes*, Vol. 4 (Wiley, New York, 1999).